Available online at www.sciencedirect.com
SCIENCE DIRECT®
Journal of Nuclear Materials 351 (2006) 247–260
journal of nuclear materials
www.elsevier.com/locate/jnucmat

Microstructural development under irradiation in European ODS ferritic/martensitic steels

R. Schäublin [a,*], A. Ramar [a], N. Baluc [a], V. de Castro [b], M.A. Monge [b], T. Leguey [b], N. Schmid [c], C. Bonjour [c]

[a] Fusion Technology-Materials, CRPP-EPFL, Association EURATOM-Confédération Suisse, 5232 Villigen PSI, Switzerland
[b] Department of Physics, University Carlos III, 28911 Leganes, Madrid, Spain
[c] Haute Ecole Valaisanne, 1950 Sion, Switzerland

Abstract

Oxide dispersion strengthened steels based on the ferritic/martensitic steel EUROFER97 are promising candidates for a fusion reactor because of their improved high temperature mechanical properties and their potential higher radiation resistance relative to the base material. Several EUROFER97 based ODS F/M steels are investigated in this study. There are the Plansee ODS steels containing 0.3 wt% yttria, and the CRPP ODS steels, whose production route is described in detail. The reinforcing particles represent 0.3–0.5% weight and are composed of yttria. The effect of 0.3 wt% Ti addition is studied. ODS steel samples have been irradiated with 590 MeV protons to 0.3 and 1.0 dpa at room temperature and 350 °C. Microstructure is investigated by transmission electron microscopy and mechanical properties are assessed by tensile and Charpy tests. While the Plansee ODS presents a ferritic structure, the CRPP ODS material presents a tempered martensitic microstructure and a uniform distribution of the yttria particles. Both materials provide a yield stress higher than the base material, but with reduced elongation and brittle behaviour. Ti additions improve elongation at high temperatures. After irradiation, mechanical properties of the material are only slightly altered with an increase in the yield strength, but without significant decrease in the total elongation, relative to the base material. Samples irradiated at room temperature present radiation induced defects in the form of blacks dots with a size range from 2 to 3 nm, while after irradiation at 350 °C irradiation induced $a_0\langle 100\rangle\{100\}$ dislocation loops are clearly visible along with nanocavities. The dispersed yttria particles with an average size of 6–8 nm are found to be stable for all irradiation conditions. The density of the defects and the dispersoid are measured and found to be about 2.3×10^{22} m^{-3} and 6.2×10^{22} m^{-3}, respectively. The weak impact of irradiation on mechanical properties of ODS F/M steel is thus explained by a lower density of irradiation induced defects relative to the density of reinforcing particles.

1. Introduction

Oxide dispersion strengthened (ODS) ferritic/martensitic steels appear to be promising candidates for the future fusion reactor. Their inherent properties, that is to say their good thermal conductivity,

* Corresponding author. Tel.: +41 56 310 40 82; fax: +41 56 310 4529.
E-mail address: robin.schaeublin@psi.ch (R. Schäublin).

0022-3115/$ - see front matter © 2006 Elsevier B.V. All rights reserved.
doi:10.1016/j.jnucmat.2006.02.005

swelling resistance and low radiation damage accumulation deriving from the base material, are further enhanced by the presence of a fine dispersion of oxide particles. They would allow in principle for a higher fusion reactor operating temperature, which improves its thermal efficiency. In effect, their strength remains higher than the base material with increasing temperature [1–3]. Their creep properties are also improved relative to the base material [4–6].

ODS steels are generally produced in two steps, the first one consisting of mechanically alloying the reinforcing particles with the base metal in the form of atomized powder, followed by a second step, or compaction, achieved generally by hot isostatic pressing. Hot extrusion is also used but leads to a strongly textured material. The oxide that is usually selected for the reinforcement is yttria (Y_2O_3), as it is more stable thermodynamically than nitrides and carbides and is one of the most stable oxides. It appears to be superior than TiO_2 or $MgAl_2O_4$. For example, the Y_2O_3 containing alloy appears slightly superior to the TiO_2 dispersion in a 13% Cr, 1.5% Mo and 2–3% Ti ferritic steel [7], and in EUROFER97 $MgAl_2O_4$ tends to remain undissolved during the mechanical alloying and form larger particles than Y_2O_3, which is detrimental to creep properties [8]. Small amounts of Ti are added for mechanical alloying in order to refine the dispersion of reinforcing oxide on reprecipitation during the hot isostatic pressing [9]. It appears that a precise control of the chemistry, and in particular the O and Ti content [10,11] but also the C content, is crucial as contamination by foreign elements during the processing has detrimental effects on the mechanical properties of the final product.

In contrast with irradiation effects in F/M steels, the effect of irradiation on ODS F/M steels is not so well known but knowledge on the topic is rapidly growing. In F/M steels, irradiation leads to strong hardening and reduction in elongation starting at the lowest doses [12] and fracture properties are strongly degraded with a shift of the ductile to brittle transition temperature (DBTT) above room temperature [13]. Damage accumulation, however, is much lesser than in other metals such as stainless steels or pure fcc metals [14]. At low doses, following both neutron and high energy proton irradiations, transmission electron microscopy reveals in F82H unidentified so-called black dots, presumably interstitial clusters, with sizes ranging from 1 to 2 nm [15]. Similar observations are made in Fe and Fe–Cr [16]. The Burgers vector of these defects seem to be $1/2\ a_0\langle 1\,1\,1\rangle$, for all of them are visible with $\mathbf{g} = \{2\,0\,0\}$ and only half of them are visible with $\mathbf{g} = \{0\,1\,1\}$ [17]. Small angle neutron scattering measurements indicate a dispersion of nanodefects with a mean size of 0.6 nm in irradiated EUROFER97 [18]. At higher doses and at about 300 °C in F82H dislocation loops with a Burgers vector $a_0\ \langle 1\,0\,0\rangle$ and sitting on $\{1\,0\,0\}$ planes appear [19] and nanocavities are observed [20]. The strong irradiation induced hardening of F/M steels is however still difficult to rationalize in terms of the damage observed in TEM. Indeed, the observable defect density and size are too low to explain it in the frame of the dispersed barrier hardening model [19].

In ODS F/M steels one of the concerns is the oxide dispersion evolution under irradiation. It appears to be relatively stable [21]. Even at 200 dpa oxide particles in MA957 ODS steel remain unchanged [22]. In DT2203Y05 irradiated to 81 dpa, however, there was a slight coarsening of the oxide particles [23], which is attributed to the higher irradiation temperature as compared to the 200 dpa irradiation or the type of oxide, yttria versus titanium oxide or mixed [21]. ODS F/M steels should present a lower damage accumulation rate than the base material because, on the first hand, oxide particles should act as trapping sites for irradiation induced defects and, on the second hand, because the mechanical alloying results in a nanostructured microstructure that also provides a high density of trapping sites such as grain boundaries [24,25]. This in turn would stabilize the mechanical properties. MA957 ODS steel irradiated at high temperatures (410–730 °C) shows indeed no significant alteration of its tensile strength, while a mere 20% hardening and a small loss of ductility are observed for irradiations performed below 500 °C [26,27]. This change is lesser than what is observed in, e.g., F82H steel [27]. The DBTT however is significantly increased but no swelling is observed [26]. This absence or strong reduction of swelling relatively to F/M steels observed in various ODS steels and for various irradiation conditions [28–30] is attributed to the high density of oxide particles acting as trapping sites.

In this work various European ODS steels based on the EUROFER97 F/M steel are considered. CRPP ODS steels were produced, with particular attention on the control of the chemistry and the microstructure during the processing. The mechanical properties were assessed and their response to irradiation to high energy protons is reported.

2. Experimental

Various ODS ferritic/martensitic steels based on EUROFER97 are considered in this study, as explained in the next paragraph. Samples were irradiated with 590 MeV protons in the PIREX facility located at the Paul Scherrer Institute, Switzerland. They were irradiated to 0.3, 1.0 and 2.0 dpa to temperatures of 40 °C and 350 °C, in the shape of flat tensile test specimen, 0.3 mm thick, 2.5 mm wide and with a gauge length of 5.5 mm. Uniaxial tensile testing was performed on an instrumented Zwick machine, allowing testing temperatures from room temperature to 1000 °C, in an Ar atmosphere to avoid oxidation. The applied strain rate was in all cases $5 \times 10^{-5}\,s^{-1}$. Transmission electron microscopy observations were conducted on a JEOL2010, LaB6, high tilt lens, operated at 200 kV. In order to reduce radioactivity and magnetism, samples were prepared from disks of 1 mm in diameter punched in the gauge length of the tensile test specimens, and inserted in a 3 mm stainless steel disk [15]. The observation conditions are those typical for F/M steels [15], with $\mathbf{g} = \{0\,1\,1\}$ as diffraction vector, and $\mathbf{g}(4\mathbf{g})$ as diffraction condition for weak beam observations.

The base material is ferritic/martensitic steel EUROFER97 which contains 8.9 wt% Cr, 1.1 wt% W, 0.47 wt% Mn, 0.2 wt% V, 0.14 wt% Ta, 0.11 wt% C and Fe for the balance. Two types of EUROFER97-based ODS steels are considered in this study. On the one hand, there are ODS variants developed by the company Plansee, Austria, in the frame of the European fusion programme. They were produced by mechanical alloying and hot isostatic pressing. The Plansee ODS containing 0.3 wt% yttria is considered here. On the other hand, there are the CRPP ODS variants. The EUROFER97 material was gas atomized and sieved to sizes below 45 μm. The yttria, the reinforcing material, was provided as a powder with particles sizes between 15 nm and 30 nm. Its structure is monoclinic, as confirmed by TEM electron diffraction patterns [31]. The sieved atomized EUROFER97 powder and the reinforcing particles were mixed in an attritor and the compaction was made following a two-step procedure. First, the powder is prepressed in order to close the porosity, thus avoiding canning and, second, the prepressed material is further compacted by hot isostatic pressing. The casts produced consist of a CRPP ODS containing 0.3 wt% yttria, 0.3% yttria and 0.3% Ti and 0.3% yttria and 1.0% Ti. In addition, a reference material was made of compacted sieved atomized EUROFER97 powder without any reinforcing material, the so-called compacted EUROFER97. In the following section the production route of the CRPP ODS material is described in detail.

2.1. Mechanical alloying

The powders of EUROFER97, yttria and/or Ti were mixed [31] by mechanical attrition at University Carlos III, Madrid, Spain, in a horizontal high speed attritor. The as-received atomized EUROFER97 powder particles present a spherical shape (Fig. 1(a)), are coated with a thin oxide layer (Fig. 1(b)) and have a martensitic structure (Fig. 1(c) and (d)) without carbides. The mechanical alloying conditions were optimized and are summarized in Table 2 of [31]. The ball milling was achieved with a ball to powder ratio of 1–15, at 800 rpm, Ar atmosphere and at room temperature during 24 h, in twelve cycles of 2 h each. These conditions were selected in order to limit particle size growth and carbon intake, while preserving an adequate mixing of the metal with the yttria and with or without the titanium. The ODS powder was processed in batches of about 100 g each. The resulting ODS yttria content is 0.27 wt% and the final ODS particle size is roughly 50 μm. Fig. 2 shows TEM micrographs of the resulting microstructure. It is nanostructured (Fig. 2(a) and (b)) and is clear of carbides and yttria particles.

The chemical composition of the resulting powders is given in Table 1. It appears that the oxygen content is increased in the atomized powder, perhaps as a result of the large surface to volume ratio of the powder. It is further increased by the ball milling process, to reach a value of 0.221 wt%. The carbon content is slightly increased by the ball milling process, by about 30% relatively to the base EUROFER97. There is a contamination in Ni, resulting from the intake from the balls and/or the container used for milling. These balls, with a diameter of 3/16 of an inch, are made out of a steel AISI 52100, a so-called high carbon chromium bearing steel. The standard chemical composition of this steel is 1.3–1.6 wt% Cr, 0.95–1.10 wt% C, 0.25–0.45 wt% Mn, 0.15–0.35 wt% Si, 0.025 wt% P, 0.025 wt% S and Fe for the balance. The balls are then certainly a source of C contamination, explaining the increase in C content of the powder, but cannot explain the Ni contamination. Ni may come

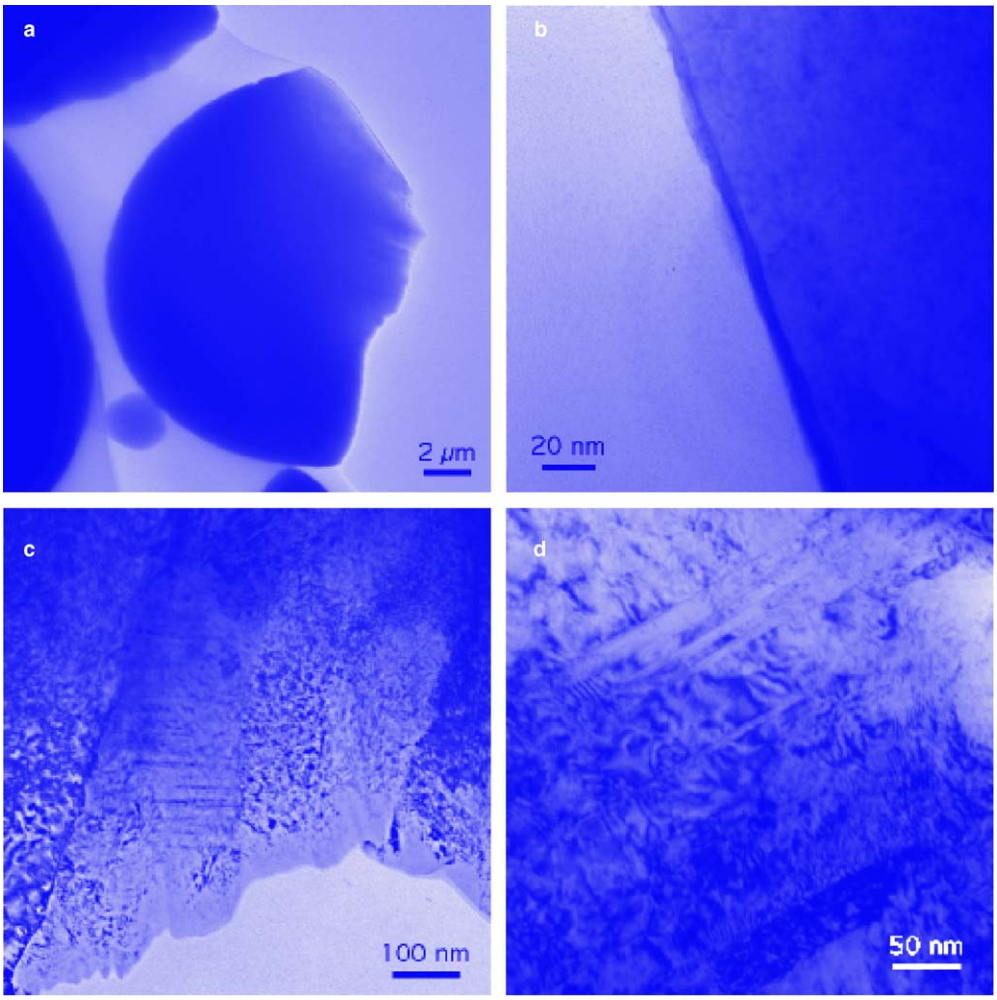

Fig. 1. TEM micrographs of the as-received atomized EUROFER97 powder particles (a), coated with a 10 nm thick layer of oxide (b), showing a martensitic lath structure (c), subdivided in thinner lathes (d). No visible carbides.

from the container. It is made out of an austenitic steel which exact composition is unknown but, as an austenitic steel, typically contains about ten weight percent of Ni, nearly twenty of Cr and much lower C content relative to EUROFER97.

2.2. Powder compaction

The processed ODS powder was sent to the Haute Ecole Valaisanne, Sion, for compaction of the ODS powder in the form of cylinders. The compaction was decomposed in two steps in order to avoid the canning that is usually used in order to simplify the process and to obtain geometrically stable ingots. The first step consists of a prepressing under 35 MPa at 1270 °C for about 7 min under a vacuum of 10^{-2} mbar. This process is meant to close the porosity in order to allow for the HIP. The canning is thus unnecessary. The powder is enclosed in a system consisting of a graphite matrix and two graphite pistons that are coated with carbon nitride in order to avoid carbon contamination. The final sample geometry is a cylinder that is 30 mm in diameter and from 6 mm to 30 mm high. This geometry allows flat tensile test specimens as well as Charpy test specimens to be extracted from one compacted specimen, as illustrated in Fig. 3. The microstructure resulting from the prepressing is martensitic (Fig. 4(a)) with thin sublathes (Fig. 4(b)), clear of carbides. Yttria particles are visible and are homogeneously distributed.

The prepressed material is then submitted to hot isosatic pressing (HIP) for one hour at 180 MPa at 1000 °C. The heating and increase in pressure before

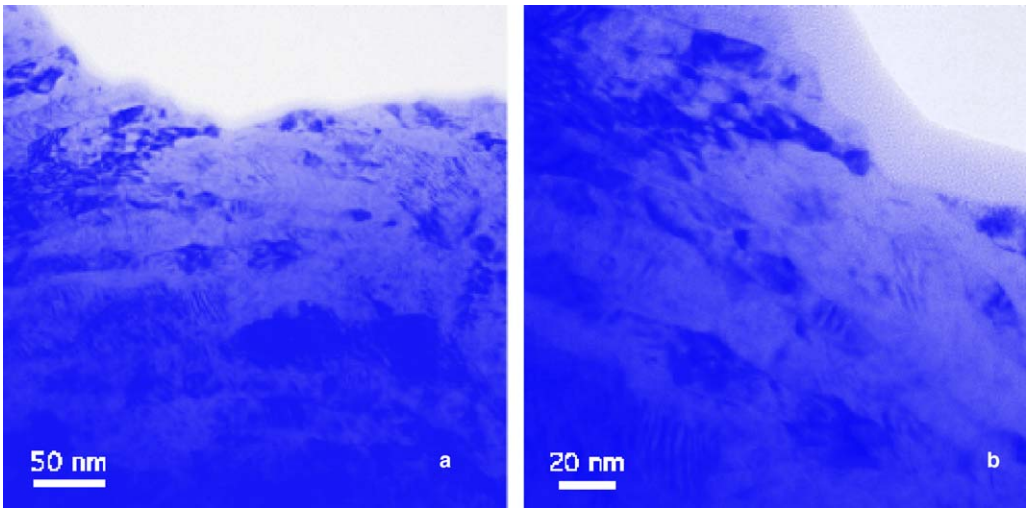

Fig. 2. TEM bright field micrographs of the CRPP ODS EUROFER97 0.3 wt% yttria powder after attrition at (a) medium and (b) high magnification, showing a nanostructured microstructure clear of carbides and yttria particles.

Table 1
Chemical composition in wt% of nominal EUROFER97, EUROFER97 powder from Studsvik, EUROFER97 powder from Studsvik sieved to sizes below 45 μm and ODS powder of below 45 μm EUROFER97 particles and 0.3 wt% yttria ball milled during 24 h

Element	EUROFER97 specifications	EUROFER97 Studsvik	EUROFER97 <45 μm	ODS powder 24 h
O	<0.01	0.0074	0.107 ± 0.002	0.221 ± 0.011
N	0.015–0.045	0.047	0.014 ± 0.002	0.029 ± 0.003
C	0.09–0.12	0.091	0.102 ± 0.002	0.136 ± 0.005
Cr	8.5–9.5	8.75	8.88 ± 0.36	8.77 ± 0.12
Mn	0.20–0.60	0.4	0.382 ± 0.019	0.376 ± 0.007
Ni	<0.005	0.036	0.015 ± 0.001	0.080 ± 0.013
Si	<0.05	0.047	0.018 ± 0.002	0.032 ± 0.006
V	0.12–0.25	0.24	0.195 ± 0.010	0.187 ± 0.009
W	1.0–1.2	1.09	1.13 ± 0.05	1.05 ± 0.04
Y	NA	NA	<0.0005	0.192 ± 0.006

Last two column analyses performed at Carlos III, Spain [31].

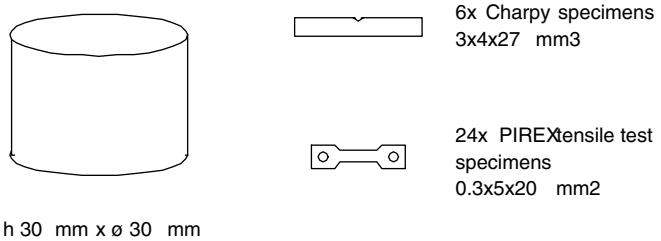

Fig. 3. Sample geometry for the production of the CRPP ODS EUROFER97 steel and the number and geometries of samples that can be extracted from it for mechanical testing.

reaching the nominal conditions take 5 h while the cooling takes 10 min to reach 700 °C, 30 min to 400 °C and 3 h to reach room temperature. Fig. 5 shows the resulting microstructure as observed in TEM. It shows prior austenite grains which size is of the order of microns containing tempered martensite (Fig. 5(a)), with martensitic lathes, a high density of dislocations and carbides (Fig. 5(b)).

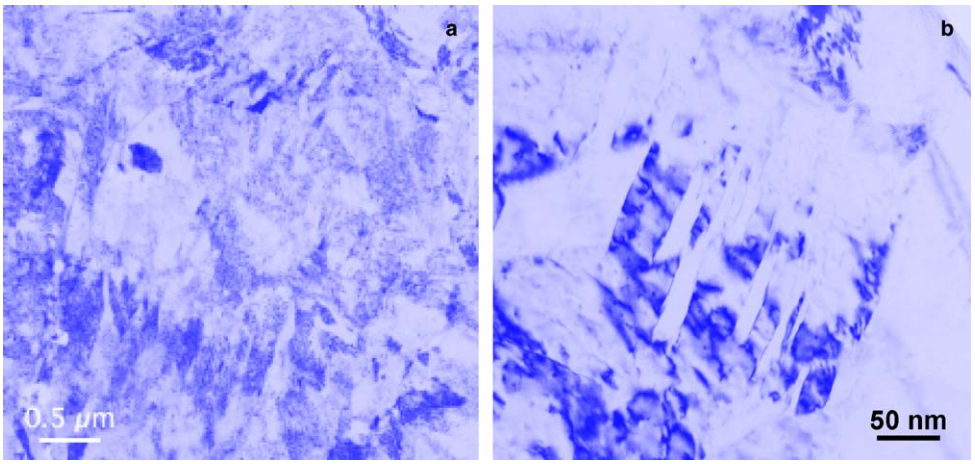

Fig. 4. TEM bright field micrograph of prepressed CRPP ODS EUROFER97 0.3% yttria, showing (a) at low magnification a martensitic structure and (b) at higher magnification thin sublathes and yttria particles. No carbides are visible.

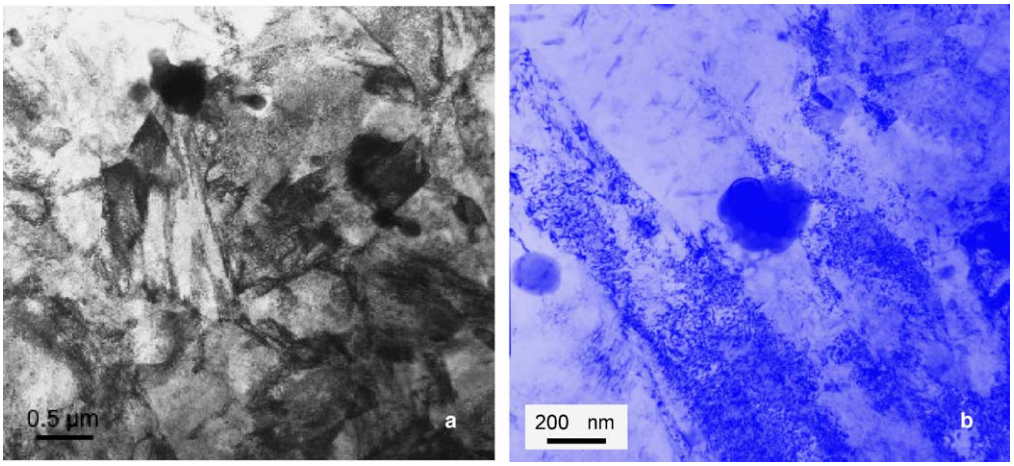

Fig. 5. TEM bright field micrograph of the HIP CRPP ODS EUROFER97 0.3% yttria, showing (a) at low magnification a tempered martensitic structure and (b) at higher magnification martensite lathes, carbides and yttria particles.

Yttria particles are visible and are observed to be homogeneously distributed. Dark field imaging reveals only part of them, indicating that they are at most semi-coherent with the matrix. Fig. 6 shows a high resolution micrograph obtained in the JEOL2010 and showing the matrix and one yttria particle in the top part. Digital power spectra displayed in the inserts and obtained in the delineated regions show that the matrix and the yttria particles are certainly not fully coherent. This indicates that the shearing of yttria particles by dislocations may be difficult.

One series of 40 plates 6 mm high and 30 mm in diameter was produced with EUROFER97 and 0.3 wt% yttria. One plate with the same geometry was produced with compacted EUROFER97 only. In addition, four plates of EUROFER97-based ODS F/M steel containing 0.3 wt% yttria and 0.3 wt% Ti and three plates of EUROFER97-based ODS F/M steel containing 0.3 wt% yttria and 1.0 wt% Ti were produced. The cylinder heights were between 10 mm and 30 mm, as illustrated in Fig. 3. The chemical composition of the materials was thoroughly assessed as a function of the processing steps.

2.3. Chemical evolution

Initially, the content in alloying elements was measured for the materials without Ti additions in

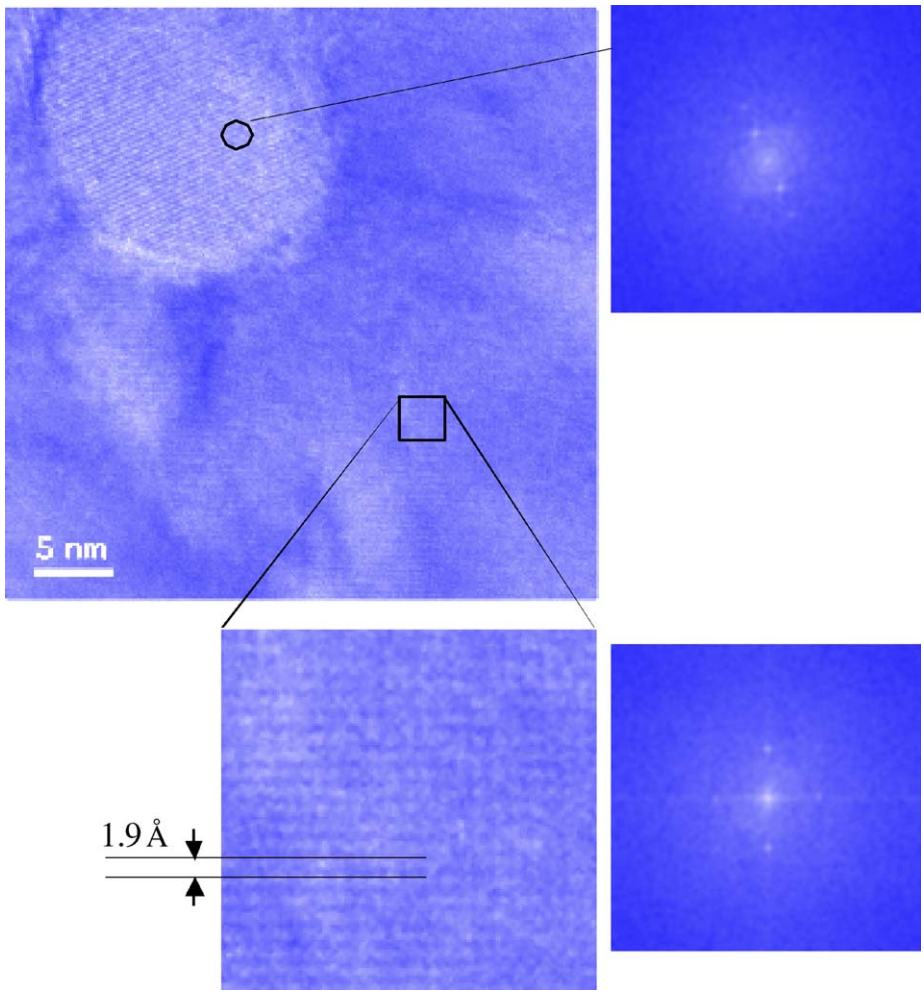

Fig. 6. HR-TEM micrograph (top left) of the HIP CRPP EUROFER97 ODS 0.3% yttria showing the matrix and one yttria particle in the top. The matrix is oriented along ⟨1 0 0⟩ as shown in the bottom left picture. The two inserts in the right show the digital power spectra obtained in the delineated regions of the micrograph, indicating that the yttria particle is not fully coherent with the matrix.

order to check the stability of the steel composition during the fabrication process (Table 1). Also, an additional compacted specimen containing 0.5 wt% yttria was measured in order to check the evolution of yttrium content with the compaction process.

The analysis on the compacted material was performed by wavelength dispersive X-ray fluorescence (WD-XRF) spectrometry. The resolution of this method is 0.01 g/100 g, that is to say that amounts lower than 1% in weight may be detected but not quantified. They are indicated as <0.01. For solid samples which surface is prepared by first a mechanical polish and second by an electrochemical polish the relative error is 5%. For powder samples the relative error is 10%–20%. Results are presented in Table 2. It appears that most of the alloying element contents remain constant during the fabrication process. The yttrium content reflects the designed amount of yttria, either 0.3 wt% or 0.5 wt%, added in the attritor for the mechanical alloying of the ODS powder.

As noted earlier the mechanical alloying process introduces Ni contamination, coming certainly from the ball milling container. It should be noted that the amount of contamination is less (0.05%) than what was measured earlier (0.08%) and reported in Table 1. The amount of Ni in the base material, however, also varies with the analysis. It ranges from less than 0.01 (Table 2) to 0.015% (Table 1). The trend being the same, that is that all the values in Table 1 values are all slightly higher than the ones in Table 2, one can nonetheless conclude that the

Table 2
Chemical composition in wt% of the atomized EUROFER97 powder (<45 μm particles), the ball milled ODS powder with 0.3 wt% yttria, the compacted samples of ball milled EUROFER97 powder only (neither yttria nor Ti additions), ODS powder with 0.3 wt% yttria and with 0.5 wt% yttria

	EUROFER97 powder	ODS 0.3% Y_2O_3 powder	EURO97 compact	ODS 0.3% Y_2O_3 compact	ODS 0.5% Y_2O_3 compact
Al	<0.01	<0.01	NA	NA	NA
Si	<0.01	<0.01	0.05	<0.01	<0.01
P	0.01	0.01	<0.01	<0.01	<0.01
S	0.02	<0.01	0.01	0.01	0.01
Ti	<0.01	<0.01	<0.01	<0.01	<0.01
V	0.20	0.19	0.19	0.19	0.20
Cr	9.10	9.00	9.10	8.90	8.80
Mn	0.41	0.40	0.41	0.41	0.39
Co	<0.05	0.34	0.12	0.12	0.17
Ni	<0.01	0.05	0.06	0.06	0.07
Cu	<0.01	<0.01	<0.01	<0.01	0.09
Y	<0.01	0.24	0.20	0.20	0.35
Nb	<0.01	<0.01	<0.01	<0.01	<0.01
Mo	0.01	0.01	<0.01	<0.01	<0.01
Ta	NA	NA	0.02	0.02	0.02
W	1.00	1.00	1.10	1.10	1.10

WD-XRF analyses performed at EMPA.

contamination by ball milling increases the Ni content by a factor of about 5.

The Co content, not measured previously, shows in Table 2 a nearly threefold increase in the compacted material, from less than 0.05% to a value ranging from 0.12% to 0.17%. The Co content of EUROFER97 as-received plates was measured to be about 0.006%, suggesting a larger Co contamination than what is deduced from the present WD-XRF measurements. This contamination comes from the ball milling process and the only possible source of contamination is the austenitic steel of the container. Note that the value of Co content in the ODS powder is odd, with 0.34%, as it is higher than the one in the compacted material. It may come from the larger error of analysis when measuring powders as compared to solid samples. The amount of Ni and Co contamination remains nearly constant with prepressing and HIP in the different materials.

In a second stage, the O, C and N content was measured for the ODS powders with Ti additions after ball milling and after compaction (prepressing + HIP). The O and N contents were quantified using hot extraction with a LECO TC-436 analyzer. The C content was quantified using hot extraction with a LECO IR-412 analyzer. The samples were first dipped into acetone followed by ethylic alcohol in order to remove any grease. Then the samples were washed in water and, finally, were dried at about 80 °C in a drier cupboard. Tables 3–5 present respectively the content in O, N and C. For each type of measurement a so-called standard from LECO company was analyzed prior to the actual measurements in order to assess the accuracy of the analysis. Three to five analyses were performed on each type of specimen.

Table 3 shows that the O content in the ball milled ODS powder is about twice the value in the as-received EUROFER97 powder (Table 1), which

Table 3
Oxygen content in wt% of the CRPP ODS powders after ball milling and after compaction (prepressing + HIP)

	Standard 0.029 ± 0.0010	ODS powder 0.3% Ti	ODS powder 1.0% Ti	EUR097 compact	ODS compact	ODS compact 0.3% Ti	ODS compact 1.0% Ti
O	0.0291	0.3380	0.2267	0.1917	0.2595	0.4281	0.3685
Δ	0.0006	0.0055	0.0054	0.0296	0.0218	0.0340	0.0173
Δ (%)	1.97	1.63	2.38	15.42	8.42	7.95	4.69

A LECO reference sample 'standard' was measured to assess the measurement precision. 'EURO97 HIP' : compacted sample of ball milled EUROFER97 powder only (neither yttria nor Ti additions). Δ: error. Hot extraction analyses performed at PSI.

Table 4
Carbon content in wt% of the CRPP ODS powders after ball milling and after compaction (prepressing + HIP)

	Standard 0.864 ± 0.009	ODS powder 0.3% Ti	ODS powder 1.0% Ti	EUR097 compact	ODS compact	ODS compact 0.3% Ti	ODS compact 1.0% Ti
C	0.8603	0.1353	0.1743	0.2076	0.1519	0.1347	0.1712
Δ	0.0066	0.0047	0.0030	0.0092	0.0060	0.0104	0.0094
Δ (%)	0.77	3.44	1.73	4.42	3.93	7.69	5.49

A LECO reference sample 'standard' was measured to assess the measurement precision. 'EURO97 HIP' : compacted sample of ball milled EUROFER97 powder only (neither yttria nor Ti additions). Δ: error. Hot extraction analyses performed at PSI.

Table 5
Nitrogen content in wt% of the CRPP ODS powders after ball milling and after compaction (prepressing + HIP)

	Standard 0.0481 ± 0.0011	ODS powder 0.3% Ti	ODS powder 1.0% Ti	EUR097 compact	ODS compact	ODS compact 0.3% Ti	ODS compact 1.0% Ti
N	0.0478	0.0586	0.0520	0.0755	0.0961	0.1136	0.1638
Δ	0.0006	0.0018	0.0029	0.0002	0.0109	0.0319	0.0045
Δ (%)	1.15	3.06	5.53	0.29	11.29	28.06	2.73

A LECO reference sample 'standard' was measured to assess the measurement precision. 'EURO97 HIP' : compacted sample of ball milled EUROFER97 powder only (neither yttria nor Ti additions). Δ: error. Hot extraction analyses performed at PSI.

in turn contains ten times the O amount of the base EUROFER97. This is due to the natural oxidization of the surfaces and the high surface to volume ratio of the powder relatively to the bulk material. The increase in O by ball milling is mainly due to the oxygen of the yttria. In addition, it appears that the O content is higher in the ball milled ODS powder containing Ti (Table 3). In effect, the O content ranges from 0.2267 wt% to 0.3380 wt% in the ODS powder with Ti additions as compared to 0.221% in the ODS powder without Ti addition (Table 1). This is due to the fact that the Ti powder added in the ball mill comes as particles with naturally oxidized surface and thus contributes to the O contamination.

In addition, Ti has a strong affinity for O and might have caught the traces of O_2 left in the Ar atmosphere of the attritor. In the final material containing additions of Ti, after pre-pressing and HIP, the O content is still higher, by about 30%. Note that in the material 'EURO97 compact', containing neither yttria nor Ti additions, there is also an increase in O content after ball milling and compaction relative to the EUROFER97 powder. This indicates that Ti might not be the only material acting as an O getter in the fabrication process. When considering the ODS material, without Ti addition, the increase in O content due to prepressing and HIP is about 15% (from 0.221% in Table 2 to 0.260% in Table 4). It shows that indeed Ti is not the only getter during the compaction process, but, it is a strong one because the O intake is larger (30%).

The carbon content, presented in Table 4, is not significantly affected by the compaction process. It remains at about 0.15%, a value similar to what was found in the ball milled powder (Table 1). Note that in the previous report it was already indicated that the ball milling process introduces C contamination due to the high carbon steel of the milling balls, which increases the C content from 0.11% of the nominal EUROFER97 to about 0.15%. These results indicate that the pre-pressing process performed with a graphite matrix and two graphite pistons is well controlled. There is no C intake from the graphite environment during prepressing, thank to the boron nitride coating of the inner surfaces of the graphitic ensemble prior to prepressing.

Note that the C content of the compacted EUROFER97 powder, containing neither yttria nor Ti additions, is 30% higher than the average value for the compacted materials. This is attributed to scatter in the C contamination level during the ball milling process.

Table 5 shows that the N content increases during the compaction process, including the pre-pressing and the HIP steps. It goes from a value after ball milling of about 0.05%, which is the content in nominal EUROFER97, showing that there is no N contamination during ball mill, to a value ranging from 0.076% to 0.16% in the compacted material. It

seems unlikely to come from the boron nitride used to coat the graphite pressing system used for pre-pressing, as boron nitride is a relatively stable compound. The N contamination during the compaction process comes certainly from the HIP step, as the vector of isostatic pressing during HIP is gaseous N (N_2). It appears that the highest values in N content are obtained in the ODS containing Ti additions, in proportion to the Ti content. This indicates that Ti is a getter of N and collects it during HIP.

3. Results

3.1. Mechanical properties

In the following the results of mechanical testing are presented. Samples of CRPP ODS material containing 0.3 wt% yttria and 0.3 wt% Ti, referenced in the following as ODS-Ti, and ODS material containing 0.3 wt% yttria only, referenced as ODS, were considered. In addition, samples of base EUROFER97, referenced as such, were also deformed following the same procedure. Fig. 7 presents their yield stress and total elongation as a function of temperature.

It appears that both ODS have, as expected, a higher yield stress than the base material, EUROFER97. The ODS, however, and despite the large data scatter, presents a higher yield stress than the ODS-Ti. With increasing temperature the values and the gap between the two materials decrease and reach the same yield stress at 600 °C.

The elongation at failure is presented in Fig. 7 right. Both ODS steels present values below 5% at room temperature, which indicates a near to fragile behaviour, while the EUROFER97 presents a practicable ductility, at 15%. With increasing temperature the elongation increases for EUROFER97 and ODS-Ti, above 450 °C, but not for the ODS. At the highest temperature EUROFER97 presents the highest elongation of all materials. The ODS-Ti presents at 600 °C a very interesting elongation, at about 17%.

Charpy tests were performed in order to assess the fracture toughness of the ODS 0.3 wt% Ti. Table 6 summarizes the result. It appears that this material is brittle up to 500 °C, the highest temperature that can be probed with the present equipment. The shift of the DBTT towards higher temperatures is a common consequence of the reinforcement of ferritic/martensitic steels [6]. Recently, however, in the EFDA programme efforts have been devoted to design a new thermal treatment to improve the fracture behaviour of the Plansee

Table 6
Absorbed energy in a Charpy impact test of a $3 \times 4 \times 27$ mm three sample of EUROFER97 based ODS steel with 0.3 wt% yttria and 0.3 wt% Ti

Test temperature (°C)	Energy absorbed (J)
28	0.20
200	0.17
400	0.38
500	0.40

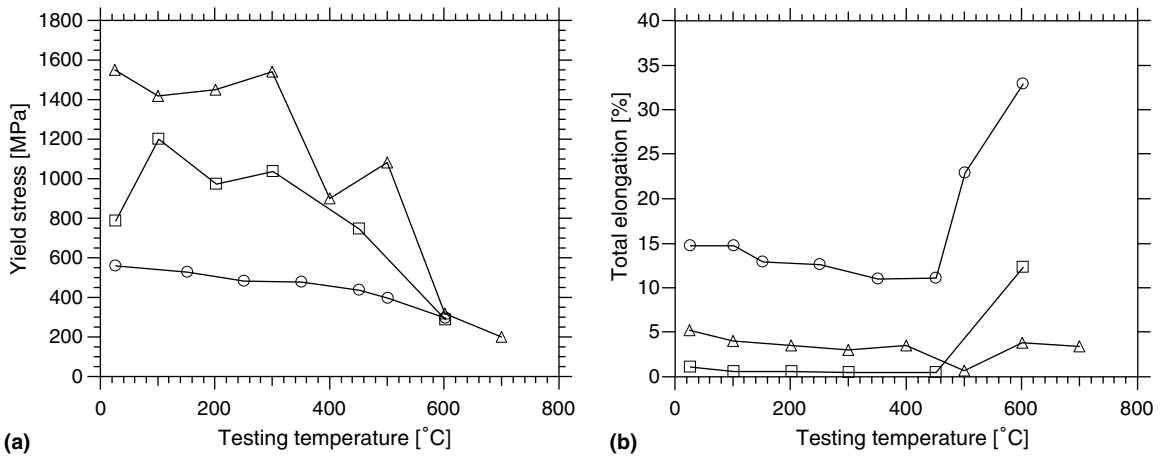

Fig. 7. Tensile yield strength (a) and total elongation (b) as a function of testing temperature of (-○-) as-received EUROFER97, (-△-) CRPP ODS EUROFER97 0.3 wt% yttria and (-□-) CRPP ODS EUROFER97 0.3 wt% yttria and 0.3 wt% Ti.

ODS. A treatment consisting of 980 °C for 30 min followed by 750 °C for 2 h resulted in a very promising shift of the DBTT from about 150 °C to about 0 °C [32].

3.2. Irradiation induced effects

Plansee ODS irradiated to 0.3, 1.0 and 2.0 dpa at 40 °C does not show a drastic change in mechanical properties (Fig. 9), as compared to the unirradiated condition (Fig. 8) [3], relative to an irradiated F/M steel. There is a mere 20% hardening, from about 900 MPa to 1.1 GPa, which stays constant with increasing dose, while the total elongation remains nearly unchanged (Fig. 9).

The CRPP ODS irradiated to 1.0 dpa at 350 °C presents some hardening relative to the unirradiated condition and a reduction in elongation by half (Fig. 10). Interestingly, this hardening is similar to the one observed in the irradiated compacted EUROFER97 (Fig. 10), indicating that the reduction in damage accumulation might be driven by the nanostructured microstructure rather than by the oxide dispersion. Indeed, a nanostructured material presents a high density of trapping sites, as grain boundaries and dislocations, that might significantly reduce the irradiation induced defect density [25]. It should be noted also that the irradiation temperature does not seem to affect the hardening. In effect, the compacted EUROFER97 shows a similar yield stress after irradiation at 40 °C and 350 °C to the same irradiation dose of 1.0 dpa (Fig. 10), while the irradiation induced microstructures are different, as explained in the next paragraph.

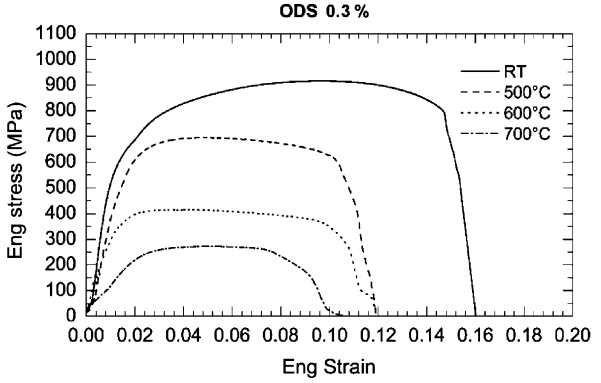

Fig. 8. Tensile test response as a function of temperature of unirradiated Plansee ODS [3].

TEM observations reveal that the oxide dispersion remains unchanged by the irradiation in Plansee ODS (Fig. 11(b)) as well as in CRPP ODS. The irradiation induced defects consist at low irradiation temperature (40 °C) of black dots (Fig. 11(a)), similar to what is observed in F/M steels for similar irradiation conditions. At 350 °C, the CRPP ODS as well as the compacted EUROFER97 present after irradiation to 1.0 dpa a structure of well developed dislocation loops (Fig. 12(a) and Fig. 13(a)), similar to what is observed in F/M steels for similar irradiation conditions. The loops have a Burgers vector $a_0\langle 1\,0\,0\rangle$ and are sitting on $\{1\,0\,0\}$ planes (Fig. 12(b)). A high density of nanocavities is observed (Fig. 13(b)) in the case of the CRPP ODS.

The dispersed barrier hardening model enables hardening due to a dispersion of obstacles to be expressed as a function of their density and size with the following relationship, $\Delta\sigma = \alpha\mu b(Nd)^{1/2}$, where α is the obstacle strength, μ the shear modulus, b the Burgers vector, N the defect density and d the defect

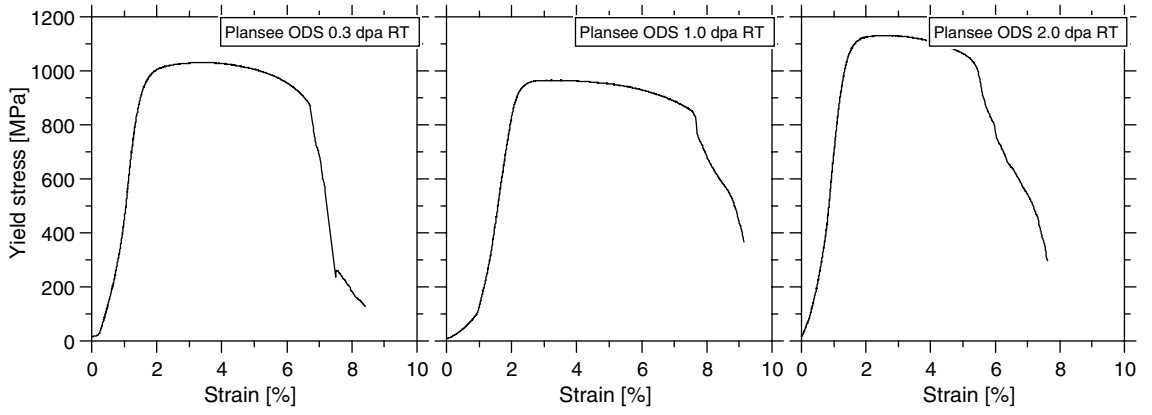

Fig. 9. Tensile test response at room temperature of Plansee ODS irradiated at 40 °C to 0.3, 1.0 and 2.0 dpa from left to right.

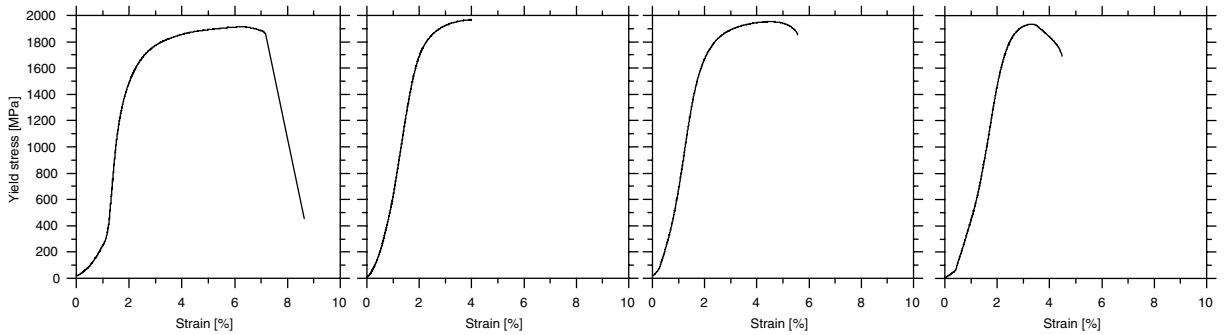

Fig. 10. Tensile test response at room temperature of CRPP ODS EUROFER97 0.3% yttria unirradiated, irradiated at 350 °C to 1.0 dpa, and compacted EUROFER97 irradiated at 350 °C to 1.0 dpa, from left to right.

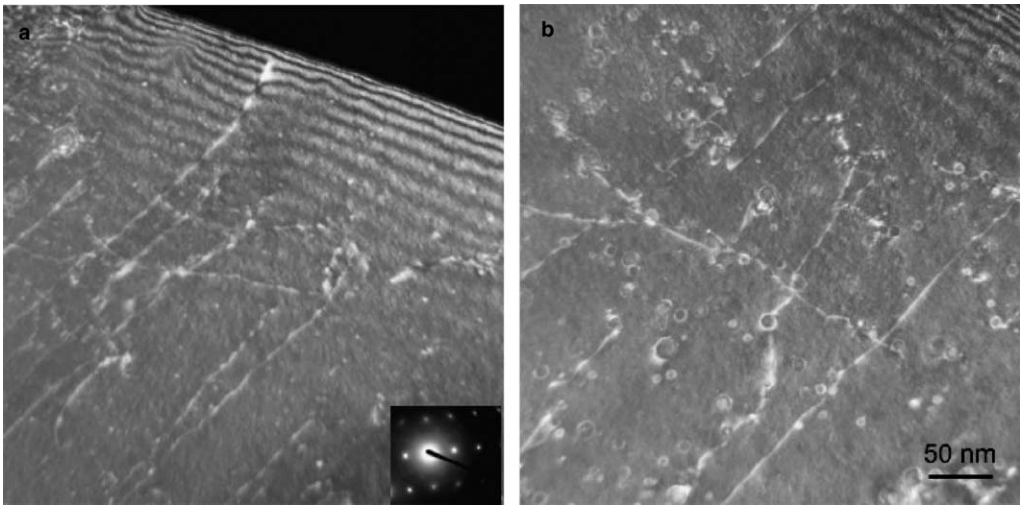

Fig. 11. TEM weak beam dark field micrographs, $\mathbf{g} = \{0\,1\,1\}$, $\mathbf{g}(4\mathbf{g})$, of Plansee ODS irradiated to 1 dpa at 40 °C, showing (a) dislocation lines and irradiation induced 'black dots' and (b) unchanged yttria particles.

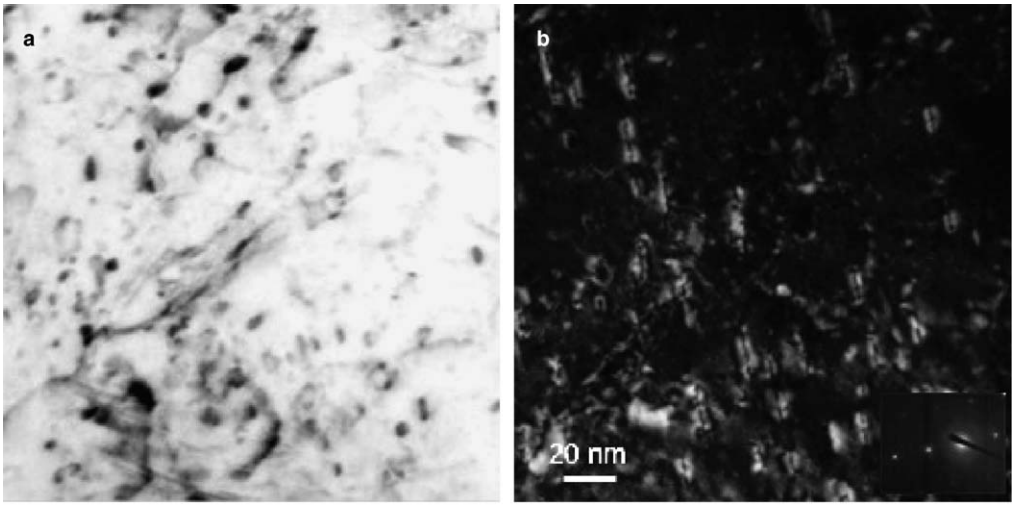

Fig. 12. TEM (a) bright field micrograph and (b) weak beam dark field micrograph, $\mathbf{g} = \{2\,0\,0\}$, $\mathbf{g}(4\mathbf{g})$, of compacted EUROFER97 irradiated to 1.0 dpa at 350 °C, showing (a) well developed dislocation loops that appear (b) to be sitting on $\{1\,0\,0\}$ planes.

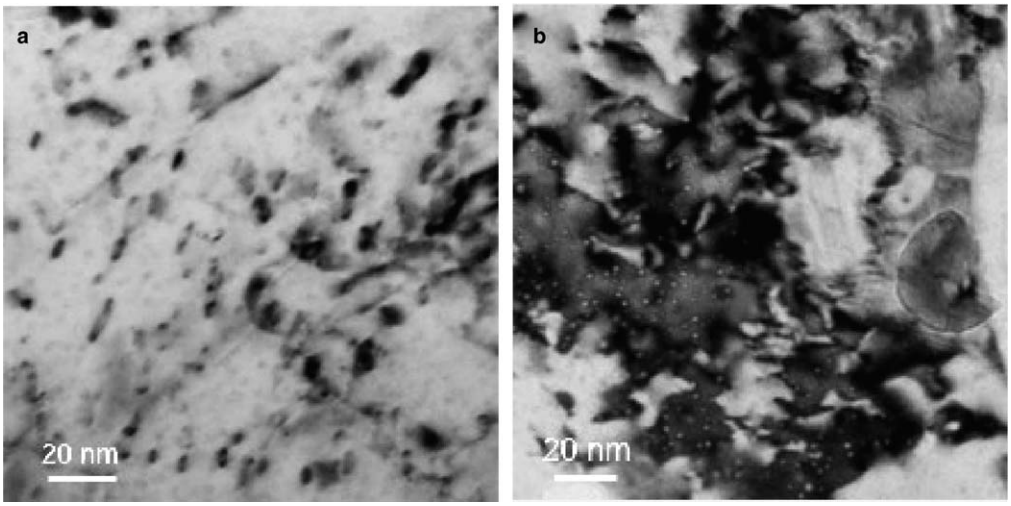

Fig. 13. TEM (a) bright field micrograph and (b) defocussed bright field micrograph of CRPP ODS EUROFER97 0.3% yttria irradiated to 1.0 dpa at 350 °C, showing (a) well developed dislocation loops and (b) nanocavities.

mean size. It should be noted that the hardening induced by the yttria particles needs to be taken into account in this description. The irradiation induced defects and the yttria particle density and size were measured in the case of Plansee ODS irradiated to 1.0 dpa at 40 °C. The visible defect density is 2.3×10^{21} m^{-3} and the mean size is about 1.5 nm. The yttria particles mean size is about 6 nm and their density, deduced from their mean size and the known total volume of yttria introduced for the mechanical alloying, is 6.2×10^{22} m^{-3}. It appears then that the visible irradiation induced defects density is less than the original yttria particle density, which explains, at least partly, the low irradiation induced hardening and negligible change in total elongation relative to a non-reinforced F/M steel.

Other reasons for the lower irradiation impact are suggested in the following. Yttria particles can act as sinks for radiation induced point defects, which would reduce the final radiation induced damage and hence the radiation impact on mechanical properties. The mechanical alloying provides also an additional source of sinks because of the larger grain boundary fraction due to the reduced grain size relative to the base material. Moreover, the tempered F/M steel retaining the morphology of the martensite will show better radiation resistance than a more deeply recrystallized material, with equiaxed grains and low dislocation density, because of its high dislocation and lath boundary densities that act as sinks for radiation defects. The latter was shown for example in irradiated MA957 [22], where regions free of dislocation and boundaries accumulated more visible defects. To summarize, it is suggested that irradiation induced defects, even those invisible that contribute to hardening [19], accumulate less in a structure that already contains defects.

4. Summary

Various types of EUROFER97-based ODS steels were considered in this study, namely a Plansee ODS EUROFER97 steel and CRPP ODS EUROFER97 steels. It appears that these ODS F/M steels show very good radiation resistance relative to the base material.

The CRPP ODS EUROFER97 steels were produced using an original route, consisting of mechanical attrition, prepressing and hot isostatic pressing. The prepressing avoids the complication of the canning process. The reinforcing particles are made of yttria and Ti was added to improve the yttria dispersion.

The study of the chemical evolution during the fabrication process of CRPP ODS EUROFER97 steel shows a steady raise in the carbon content only during the process of milling. This carbon contamination is due to the balls used for grinding. The steady raise in the amount of oxygen is due to the oxygen trapped in the attritor mill during the powder charging process. In the case of addition of Ti an additional contamination by N is observed, acquired during the HIP process.

Tensile and Charpy tests were carried out on the specimens of compacted EUROFER97, ODS and ODS-Ti. Both ODS 0.3% yttria and ODS 0.3% yttria with 0.3% Ti show a raise of 30–40% in the yield strength relative to the base material, but with a decrease in the total elongation. ODS-Ti is shown to be brittle up to 500 °C. Ti addition improves ductility of the ODS steel at high temperatures.

Irradiation to low doses at 40 °C and 350 °C of the ODS steels does not induce a large change in the tensile properties. Plansee ODS shows a mere 20% hardening without change in ductility. CRPP ODS shows nearly no hardening while there is some change in the ductility. The irradiation induced defects are typical of the ones observed in F/M steels. The shallow impact of irradiation on ODS F/M steels is explained by the fact that the amount of dispersoid is found to be higher than the density of irradiation induced defects.

Acknowledgements

EFDA is thanked for financial support. The Paul Scherrer Institute is acknowledged for the overall use of the facilities.

References

[1] D.K. Mukhopadhyay, F.H. Froes, D.S. Gelles, J. Nucl. Mater. 258–263 B (1998) 1209.
[2] G.R. Romanoski, L.L. Snead, R.L. Klueh, D.T. Hoelzer, J. Nucl. Mater. 283–287 A (2000) 642.
[3] R. Schäublin, T. Leguey, P. Spätig, N. Baluc, M. Victoria, J. Nucl. Mater. 307–311 (2002) 778.
[4] S. Ukai, M. Harada, H. Okada, M. Inoue, S. Nomura, S. Shikakura, K. Asabe, T. Nishida, M. Fujiwara, J. Nucl. Mater. 204 (1993) 65.
[5] V.V. Sagaradze, V.I. Shalaev, V.L. Arbuzov, B.N. Goshchitskii, Yun Tian, Wan Qun, Sun Jiguang, J. Nucl. Mater. 295 (2&3) (2001) 265.
[6] R. Lindau, A. Möslang, M. Schirra, P. Schlossmacher, M. Klimenkov, J. Nucl. Mater. 307–311 (2002) 769.
[7] J.J. Huet, Sintered Metal–Ceramic Composites, in: Proceedings of the Third International School on Sintered Materials, Elsevier, Amsterdam, Netherlands, 1984, p. 197.
[8] C. Cayron, E. Rath, I. Chu, S. Launois, J. Nucl. Mater. 335 (2004) 83.
[9] S. Ukai, S. Mizuta, M. Fujiwara, T. Okuda, T. Kobayashi, J. Nucl. Sci. Technol. 39 (7) (2002) 778.
[10] S. Ohtsuka, S. Ukai, M. Fujiwara, T. Kaito, T. Narita, J. Nucl. Mater. 329–333 (2004) 372.
[11] S. Ohtsuka, S. Ukai, M. Fujiwara, T. Kaito, T. Narita, J. Phys. Chem. Solids 66 (2005) 571.
[12] P. Spätig, R. Schäublin, S. Gyger, M. Victoria, J. Nucl. Mater. 258–263 (1998) 1345.
[13] J. Rensman, H.E. Hofmans, E.W. Schuring, J. van Hoepen, J.B.M. Bakker, R. den Boef, F.P. van den Broek, E.D.L. van Essen, J. Nucl. Mater. 307–311 (2002) 250.
[14] M. Victoria, N. Baluc, C. Bailat, Y. Dai, M.I. Luppo, R. Schäublin, B.N. Singh, J. Nucl. Mater. 276 (1–3) (2000) 114.
[15] R. Schäublin, M. Victoria, J. Nucl. Mater. 283–287 (2000) 339.
[16] M.I. Luppo, C. Bailat, R. Schäublin, M. Victoria, J. Nucl. Mater. 283–287 (2000) 483.
[17] R. Schäublin, M. Victoria, in: Proc. of Mat. Res. Soc. Symp. Microstructural Processes in Irradiated Materials, G.E. Lucas, L. Snead, M.A. Kirk, Jr., R.G. Elliman (Eds.), 650, 2001, p. R1.8.1.
[18] P. Spätig, R. Schäublin, N. Baluc, J. Kohlbrecher, M. Victoria, J. Nucl. Mater. 329–333 (2004) 289.
[19] R. Schäublin, D. Gelles, M. Victoria, J. Nucl. Mater. 307–311 (2002) 197.
[20] X. Jia, Y. Dai, J. Nucl. Mater. 318 (2003) 207.
[21] S. Yamashita, N. Akasaka, S. Ohnuki, J. Nucl. Mater. 329–333 (2004) 377.
[22] D.S. Gelles, Fusion Reactor Materials Semiannual Progress Report for the Period Ending March 31, 1994, DOE/ ER-0313/16, 1994, p. 146.
[23] P. Dubuisson, R. Schill, M. Hugon, I. Grislin, J. Seran, Effect of Radiation on Materials, in: Proc. of 18th International Symposium, ASTM STP 1325, 1999, p. 882.
[24] N. Nita, R. Schäublin, M. Victoria, J. Nucl. Mater. 329–333 (2004) 953.
[25] N. Nita, R. Schäublin, M. Victoria, R.Z. Valiev, Philos. Mag. 85 (1) (2005) 723.
[26] M.L. Hamilton, D.S. Gelles, R. Lobsinger, G.D. Jonhson, W.F. Brown, M.M. Paxton, A.J. Puigh, C.R. Eiholzer, C. Martinez, M.A. Blotter, Report on the Fabrication Technological Development of the Oxide Dispersion Strengthened Alloy MA957 for Fast Reactor Applications, #PNNL-13168, 2002, PNL, Richmond, WA.
[27] A. Alamo, V. Lambard, X. Averty, M.H. Mathon, J. Nucl. Mater. 329–333 (2004) 333.
[28] N. Akasaka, S. Yamashita, T. Yoshitake, S. Ukai, A. Kimura, J. Nucl. Mater. 329–333 (2004) 1053.
[29] I.S. Kim, J.D. Hunn, N. Hashimoto, D.L. Larson, P.J. Maziasz, K. Miyahara, E.H. Lee, J. Nucl. Mater. 280 (2000) 264.
[30] H. Kinoshita, N. Akasaka, H. Takahashi, M. Itoh, S. Onose, J. Nucl. Mater. 179–181 A (1991) 722.
[31] V. de Castro, T. Leguey, M.A. Monge, A. Munoz, R. Pareja, D.R. Amador, J.M. Torralba, M. Victoria, J. Nucl. Mater. 322 (2003) 228.
[32] R. Lindau, European Fusion Development Agreement, Technological Programme, Report on task TW3-TTMS.